IEEE Access
Multidisciplinary ⋮ Rapid Review ⋮ Open Access Journal

Received 21 November 2023, accepted 12 December 2023, date of publication 19 December 2023,
date of current version 29 December 2023.

Digital Object Identifier 10.1109/ACCESS.2023.3344160

RESEARCH ARTICLE

Investigation on Quality Prediction Algorithm in Ultrasonic Metal Welding for Multilayered Cu for Battery Cells

HYOJUN CHOI[1,2], SEUNGMIN SHIN[3], DONG-YOON KIM[1,2], JIYONG PARK[1], DONGCHEOL KIM[1], SEUNG HWAN LEE[2], AND JIYOUNG YU[1]

[1]Advanced Joining and Additive Manufacturing Research and Development Department, Korea Institute of Industrial Technology, Yeonsu-gu, Incheon 21999, Republic of Korea
[2]Department of Mechanical Convergence Engineering, Hanyang University, Seoul 04763, South Korea
[3]Welding Design Team, LG Energy Solution, Daejeon 34122, Republic of Korea

Corresponding authors: Jiyoung Yu (willow@kitech.re.kr) and Seung Hwan Lee (seunghlee@hanyang.ac.kr)

This work was supported in part by the Ministry of Trade, Industry and Energy, South Korea, under Grant 1415185588; and in part by the Korea Institute of Industrial Technology under Grant KITECH-EH230007.

ABSTRACT This study focuses on common batteries used in electric vehicles, which are composed of cells grouped into modules and stacked to form a battery pack. Ultrasonic metal welding (UMW) is employed to bond these cells, and ensuring a reliable weld quality by inspection is crucial for maintaining the performance and stability of batteries. Currently, the quality of UMW in battery cells is assessed through sample unit-based T-peel tests and visual inspection, methods that suffer from reduced productivity and increased costs due to their destructive nature. This research introduces an algorithm designed to predict weld quality by analyzing welding process signals of the UMW process, specifically the bonding between 8-μm-thick Cu foil and 0.2-mm-thick nickel-plated copper strip materials used in battery cell manufacturing. To achieve quality prediction, current and voltage signals from the welder, as well as the displacement signal of the welded part are used. A UMW system was constructed, incorporating a current sensor, a voltage sensor, and a linear variable displacement transducer (LVDT) for measuring these signals. The study further derives welding energy from the current and voltage signals, analyzes changes in the behavior of the sonotrode during welding using the LVDT sensor, and employs data analysis to derive feature variables. These variables are then used in a machine learning-based classification model. Ultimately, the study develops and evaluates a support vector machine (SVM)-based algorithm for real-time UMW quality determination. The algorithm achieves a high classification accuracy of 98%, showcasing its effectiveness in predicting the quality of ultrasonic metal welding in the battery manufacturing process.

INDEX TERMS Ultrasonic metal welding, monitoring, sensor, knurl depth, support vector machine.

I. INTRODUCTION

In recent years, policies targeting greenhouse gas emissions have been introduced to reduce environmental pollution from transportation through the widespread deployment and expansion of renewable energy sources [1], [2], [3]. As a result, the demand for hybrid and full electric vehicle (EV) models is rapidly increasing in the e-mobility industry [4], [5]. Today, the energy density of lithium-ion technology-based batteries is directly related to the performance of the battery, and an improvement in battery performance leads to an increase in the driving range of EV drivetrains. Accordingly, technology development is focused on improving the performance of batteries, a key component of EV drivetrains [6], [7], [8], [9], [10], [11], [12], [13]. Typically, EV batteries are made of single cells combined into modules, which are then stacked to form a battery pack [14]. Battery cells have a foil-to-tab structure, in which multilayered foils and a tab are connected, and they are mainly joined by resistance spot welding, ultrasonic welding, or laser

The associate editor coordinating the review of this manuscript and approving it for publication was Jingang Jiang.

welding [15]. As such, foil-to-tab welding is directly related to the performance, efficiency, and safety of the battery, and it is important to ensure the weld quality of the foil-to-tab welds. Therefore, effective welding and joining process technologies that can produce stable quality foil-to-tab joints are needed to improve the performance and safety of batteries. Ultrasonic metal welding (UMW) is solid-phase welding that uses high-frequency ultrasonic energy and has been widely applied in battery cell assembly as a suitable technology for battery cell welding because it is less material dependent and can minimize intermetallic compound formation and energy losses in the contact area [16], [17], [18], [19]. As the geometry of the sonotrode and anvil is designed for the UMW process according to the material combination, there are no standardized guidelines for the weld quality of a multilayer UMW process [20]. Nonetheless, a T-peel test based on a common industry standard is used to evaluate the weld quality of UMW processes [21]. Mechanical testing with off-line visual inspection such as this has the disadvantage of requiring skilled operators and having a lower productivity due to time loss. Therefore, the battery manufacturing process used to join battery cells and modules requires the development of in-situ quality monitoring and inspection techniques to ensure weld quality.

As UMW is typically performed over a short period of time (0.1 - 1.0 s) and utilizes thin plates that are only a few μm thick, therefore, there are limitations to visual quality inspections. To overcome the limitations of visual quality inspections, some research has been conducted on non-destructive testing techniques that use ultrasonic process parameters (e.g., welding time, pressure, and amplitude) and measured factors (e.g., current and voltage output from the welder, displacement of the weld, and temperature) to predict and inspect weld quality. Samir et al. [22] used an experimental design method based on the response surface method to establish the relationship between the three variables of welding pressure, welding time and vibration amplitude and the three output values of power, force and energy in aluminum UMW. In addition, research on LDC-based integrative eddy current non-destructive testing method is being conducted to improve the technology of non-destructive testing [23]. Balz et al. [24] used a k-type thermocouple, a high-speed camera, and a laser Doppler vibrometer (LDV) to measure the temperature and power at the weld and the vertical displacement of the sonotrode. Then, based on a comparative analysis between the measured data and the weld quality, they showed that the aforementioned three external sensors were suitable options for process monitoring. In a study by Lee et al. [25], the welder's power and sonotrode's displacement generated during ultrasonic welding were measured using a sensor embedded in the welder and a linear variable displacement transducer (LVDT) sensor. They used the measured welding time results to classify the levels of contamination on the material surface into three classes. Ma and Zhang [26] performed ultrasonic welding on a combination of three 0.2 mm and one 0.8 mm sheets of Cu, and derived the displacement-time curve using the clamping direction of the sonotrode as measured by a high-frequency sensor and monitored the plastic deformation and welding quality. Furthermore, the microstructure was analyzed using scanning electron microscopy (SEM) and electron backscatter diffraction (EBSD), and the relationship between the displacement signal and the plastic deformation and microstructural properties of the material was explained. In the study by Guo et al. [27], a power meter, a frequency sensor, and an LVDT sensor were used to measure the power and frequency of the welder and the thickness change of the material due to welding, which were then divided into eight parts to extract features as input for weld quality prediction. They also selected ten feature points based on the processed data and developed a weld quality prediction model based on the SPC-M algorithm. Despite various studies on the correlations between weld quality and diverse variables using external sensors, there is still a lack of research on a weld quality inspection system that quantifies the correlation between process variables and T-peel strength for the UMW process and considers welding power and the sonotrode's behavior.

This study was conducted to develop a weld quality monitoring technique for battery cells using process parameters of the UMW process. For this purpose, we used multilayered 8-μm-thick Cu foil and 0.2-mm-thick nickel-plated copper strip materials and designed a system that can monitor process signals in real-time using current, voltage, and LVDT sensors. The LVDT signal was used to analyze the knurl depth displacement during the welding time, and the current and voltage signals were used to compare the output energy based on the weld quality. We obtained features from LVDT and power signals and proposed a weld quality prediction algorithm using a Support Vector Machine (SVM)-based classification model.

II. EXPERIMENTAL PROCEDURE

A. EXPERIMENTAL SETUP

For the welding experiments, we used 8-μm-thick 99.99 (wt.%) pure Cu foil and a 0.2-mm-thick nickel-plated copper strip, which were applied to pouch-type battery cells. The size of the test sheet was 50 mm long and 20 mm wide. As for the welding method, we performed welding by placing one sheet of the nickel-plated copper strip on the anvil side and 40 sheets of Cu foil in an overlapping form on the sonotrode side, to which vibration was applied, as shown in Fig. 1.

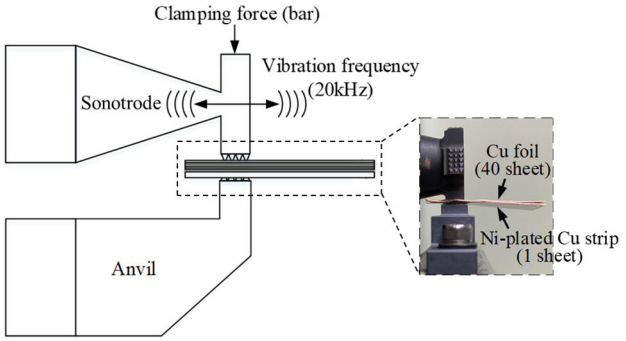

FIGURE 1. Joint type used in the experiments.

For a stable welding of the multilayered Cu foil and the nickel-plated copper strip, the sonotrode and anvil in this experiment were fabricated in the shape shown in Fig. 2.

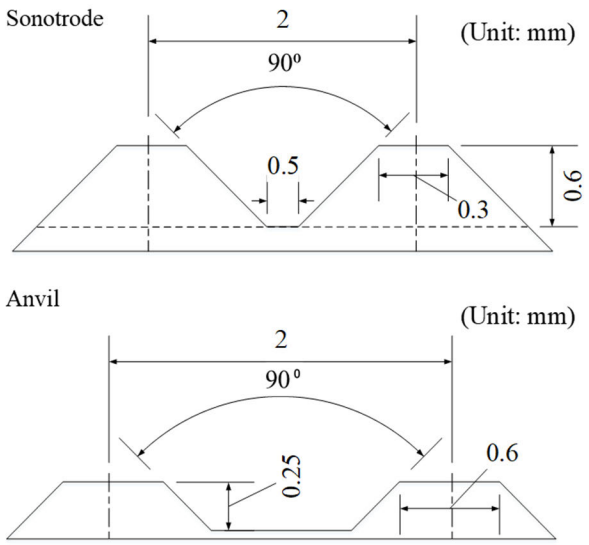

FIGURE 2. Shape of sonotrode and anvil.

An ultrasonic metal welder (FM-20) developed by KOR-MAX SYSTEM was used, which has a frequency of 20 kHz and a power specification of 3 kW. As for the experimental conditions, we selected the welding time, amplitude, and clamping force as input variables, as shown in Table 1, and conducted the experiments with four different welding times, three levels of amplitude, and four levels of clamping force. Using a full factorial design, we conducted all experiments twice with 48 experimental conditions.

TABLE 1. Welding conditions.

Factor	Levels
Welding time (s)	0.3, 0.5, 0.7, 0.9
Amplitude (%)	80, 90, 100
Clamping force (bar)	3, 4, 5, 6

For the quality inspection of ultrasonic welds, the mechanical strength was evaluated by a T-peel test using a tensile testing machine with a 500 N load cell. The travel speed was set to 50 mm/min as shown in Fig. 3, and the maximum load derived during the T-peel test was used as a measure of the welding performance.

B. SENSOR SYSTEM

The LVDT sensor used in this study is a contact-type sensor developed by ORIGIN, and its detailed specifications are shown in Table 2. The current and voltage probes used with the LVDT sensor are TT-SI 8071 developed by Testec Elektronik and CP8030 developed by CYBERTEK, respectively, and their detailed specifications are shown in Table 3.

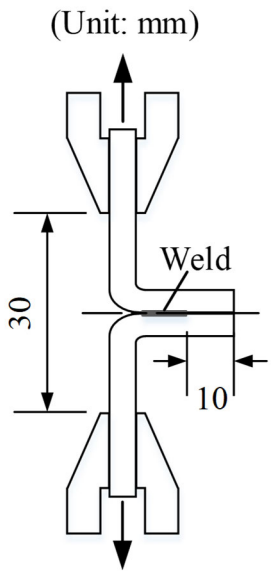

FIGURE 3. Schematic diagram of T-peel test method for weld performance evaluation.

TABLE 2. Specifications of LVDT sensor and LVDT voltage module.

LVDT sensor		LVDT voltage module	
Ranges (mm)	14 (±7)	Power requirements	±5 Vdc, ac 50Hz/60Hz at 50mA
Repeatability (mm)	0.001	Output voltage (Vdc)	±5
Frequency (Hz)	50 - 10 k	Frequency range (Hz)	10 k

TABLE 3. Specifications of current probe and voltage probe.

Current probe		Voltage probe	
Maximum continuous current	30 A	Max. DC + AC peak	±7000 V
		Bandwidth	100 MHz
Bandwidth	50 MHz	Rise time	≤ 3.5 ns
Range	50 A / 5 A	accuracy	±2%
Current Transfer Ratio	1 V / A (5 A) 0.1 V / A (30 A)	Attenuation	100 × / 1000 ×
		Bandwidth limit	≥ −3dB@5 MHz

C. SYSTEM CONFIGURATION USING SENSOR SIGNALS DURING ULTRASONIC METAL WELDING PROCESS

To measure the displacement of the sonotrode using the LVDT sensor, we designed and mounted a jig on the front side of the ultrasonic welder and placed the LVDT sensor on top

of the sonotrode, as shown in Fig. 4. For a precise knurl depth measurement, we mounted the LVDT sensor at a position at which the sonotrode and the anvil would touch each other as much as possible during welding. The connected current and voltage probes for measuring the ultrasonic welding signal are shown in Fig. 5. The voltage probe was connected to the positive and negative terminals of the secondary output terminal inside the welder controller, and the clamp-type current probe was connected to the positive terminal.

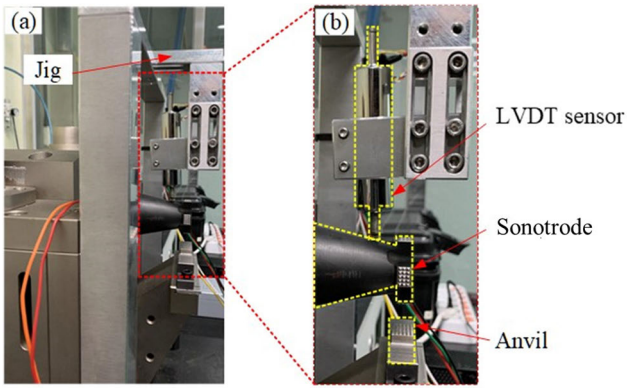

FIGURE 4. The (a) jig and (b) LVDT sensor mounting location.

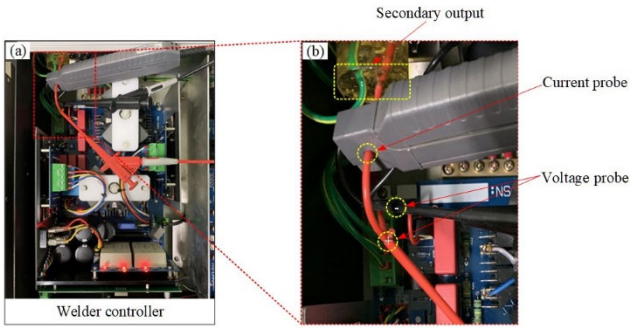

FIGURE 5. The position of (a) the inside of the controller and (b) the current/voltage sensor connection for the ultrasonic welding signal measurement.

Figure 6 shows a final signal measurement system constructed for UMW monitoring. In this system, the value of the knurl depth measured through the LVDT voltage module mounted on the front of the welder is converted into a voltage value and measured by the collection of real-time data on the data acquisition system (DAQ). Moreover, the current and voltage signals of the UMW are measured by collecting real-time data through the DAQ from the current and voltage probes connected to the secondary output terminal inside the welder controller. The data measured in real-time are sent from the DAQ to the monitoring PC through LAN communication.

III. RESULTS AND DISCUSSION

A. WELD QUALITY CLASSIFICATION

In the case of battery cells, there is currently no standard for weld quality for the UMW process because the shapes of the sonotrode and anvil are designed according to the material combination. The weld quality values obtained from the welding tests in this study can be categorized into three main weld quality types, as shown in Table 4: insufficient welding (IW), sufficient welding (SW), and excessive welding (EW). The quality grade of IW indicates that the weld is good in appearance, but the weld strength is below 40 N, and the fracture mode is the interfacial fracture or partial interfacial fracture mode in which the Cu foil is not bonded to the nickel-plated copper strip at the weld. The quality grade of SW indicates that the specimen is good in appearance, the weld strength is above 40 N, and the fracture mode is fully adhered with tearing, whereby the Cu foil is completely bonded to the nickel-plated copper strip at the weld, but below, the lower part of the weld is torn in a wavy shape. The quality grade of EW indicates that, in the appearance of the weld, discoloration of the Cu foil occurs due to excessive welding energy applied to the weld, and the weld strength varies greatly between below and above 40 N. The fracture mode in this quality grade is not consistent. For example, the lower part of the weld may break, or a fracture may occur in the form of a button fracture.

FIGURE 6. Ultrasonic metal welding monitoring system.

B. WELDABILITY EVALUATION

Figure 7 shows the weld lobe area, which is based on the mean value of the maximum strength values obtained by performing the experiment twice according to the weld quality conditions shown in Table 4. IW was mostly observed under a clamping force of 3 bar. However, under the welding time condition of 0.9 s, EW was observed due to a discoloration of the Cu foil caused by the high welding energy, although the strength value exceeded 40 N. EW was also observed under a clamping force of 4 – 6 bar and welding time of 0.7 – 0.9 s. SW was observed under the following welding conditions: clamping force of 4– 6 bar and welding time of 0.3 – 0.5 s. Therefore, it was confirmed within the experimental domain of this study that a good weld quality can be secured under conditions in which the clamping force is above 3 bar and the welding time is below 0.5 s.

C. SENSOR SIGNAL PROCESSING

1) WELDING ENERGY FROM CURRENT AND VOLTAGE SIGNALS

Using the developed measurement system, we measured the current and voltage signals during the UMW process in real

TABLE 4. Weldability evaluation standards.

Description	Load(N)	Discoloration	Failure mode	Fracture appearance
Insufficient welding	< 40	X	Interfacial	
			Partial interfacial	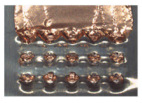
Sufficient welding	40 <	X	Fully adhered with tearing	
Excessive welding	< 40 or 40 <	O	Fully adhered with tearing	
			Fully adhered circumference fracture with tearing	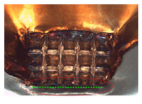
			Button	

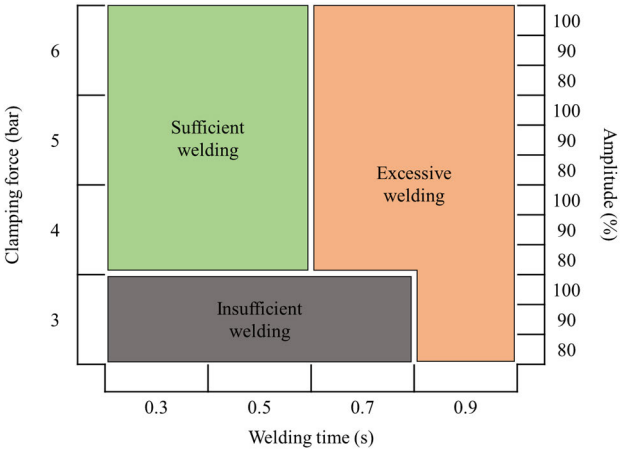

FIGURE 7. Weld lobe region.

time. The signals of the measured raw data are shown in Fig. 8, and the data were acquired at a sampling rate of 60 kHz over 2 s.

We performed data processing to derive the output energy from the acquired raw data. First, as shown in Fig. 9, the power signal that changes according to the welding time was represented in the form of a pattern using Eq. (1).

$$p(t) = i(t) \times v(t)\,[W] \tag{1}$$

Subsequently, the median filter was applied to denoise the calculated power signal. As for the median filter used in this

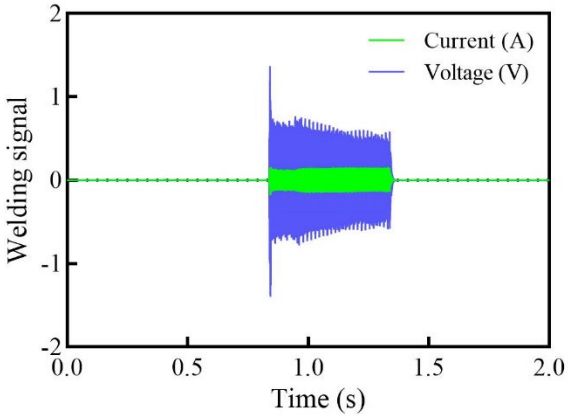

FIGURE 8. Ultrasonic metal welding current, voltage signals.

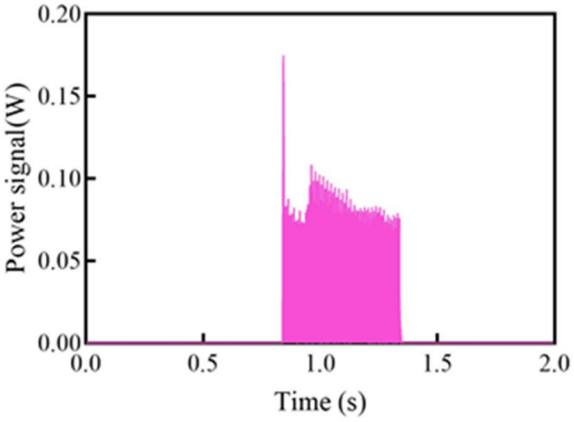

FIGURE 9. Power signal according to welding time.

study, we calculated the minimum value MIN(N(Pn)) and the maximum value MAX(N(Pn)) within the predetermined window and then calculated MEDIAN(N(Pn)) using Eq. (2). Then, moving by a window size, we repeated the above process. The window size we selected and used in this case was 50.

$$MEDIAN = \frac{MIN(N(P_n)) + MAX(N(P_n))}{2} \tag{2}$$

By integrating the power signal for which the data has been processed, as shown in Eq. (4), the output energy during the welding time can be derived, as shown in Fig. 10.

$$w(t) = \int_{t_2}^{t_2} p(t)\,dt\,[J] \tag{3}$$

2) KNURL DEPTH DISPLACEMENT FROM LVDT SIGNALS

The LVDT signal was measured in real-time with a sampling rate of 60 kHz using the knurl depth measurement system we built. As the raw data of the LVDT signal is output in the form of ±5V in the analog mode, it needs to be converted into displacement. The measurement range specification of the LVDT sensor used in this study is ±7 mm, so a gain value of 1.4 divided by 5 V was multiplied by the raw data.

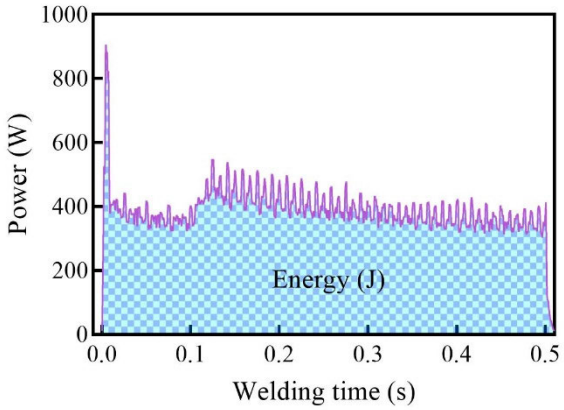

FIGURE 10. Welding energy during welding time.

Figure 11 shows the signal pattern of the LVDT converted into displacement.

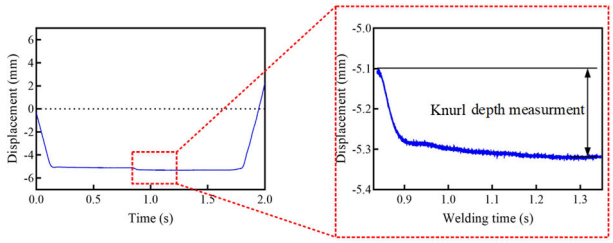

FIGURE 11. LVDT signal behavior during welding time.

Furthermore, a median filter was used to remove the noise from the LVDT signal, and in order to derive information on the changes in the knurl depth during the welding time, we ensured that the welding time of the LVDT signal started at 0 s. The displacement at 0 s was then corrected to 0 mm, as shown in Fig. 12, so that the data could be output.

D. ULTRASONIC METAL WELDING QUALITY PREDICTION MODEL USING SENSOR

1) FEATURE EXTRACTION

Figure 13 shows the growth pattern of the knurl depth according to the weld time, which is divided by the weld quality and step. Step 1 shows the growth pattern of the knurl depth from the beginning of welding to 0.1 s, while step 2 shows it from 0.1 s to 0.2 s. Finally, step 3 shows the growth pattern of the knurl depth after 0.2 s until the end of welding. IW shows a rapid growth of the knurl depth during step 1, followed by almost no change starting from step 2. However, even after step 1, during which the knurl depth grew rapidly, SW and EW show a pattern of continual growth until step 3. However, EW shows a relatively large fluctuation in the growth pattern of the knurl depth after stage 1 compared with SW.

Therefore, in this study, we analyzed the growth pattern of the knurl depth and selected the feature variables, as shown in Fig. 14. For step 1 of the growth pattern, the peak (X1) value of the knurl depth was selected, and for step 2, the peak (X2), standard deviation (std, X3), and mean (X4) values of

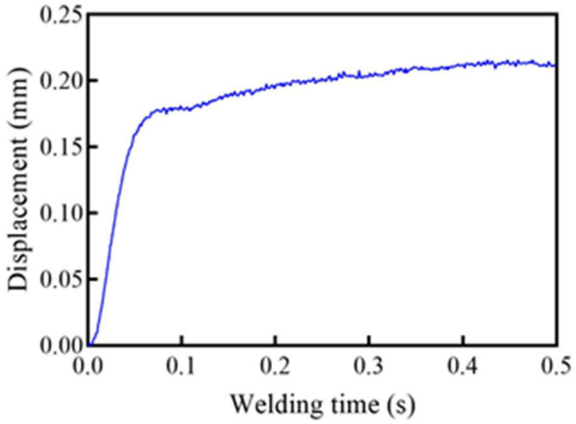

FIGURE 12. Processed LVDT signal according to welding time.

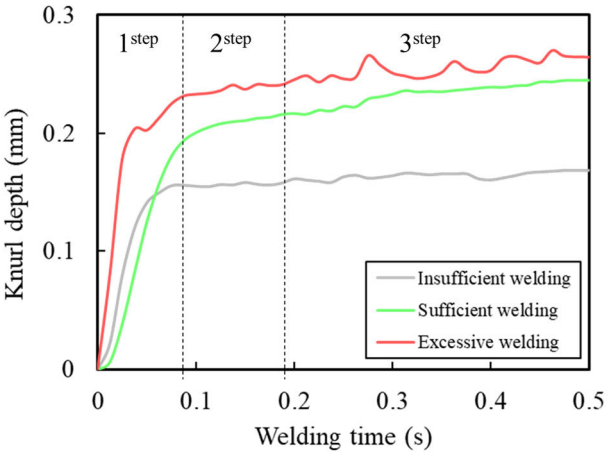

FIGURE 13. Knurl depth growth pattern according to weld quality.

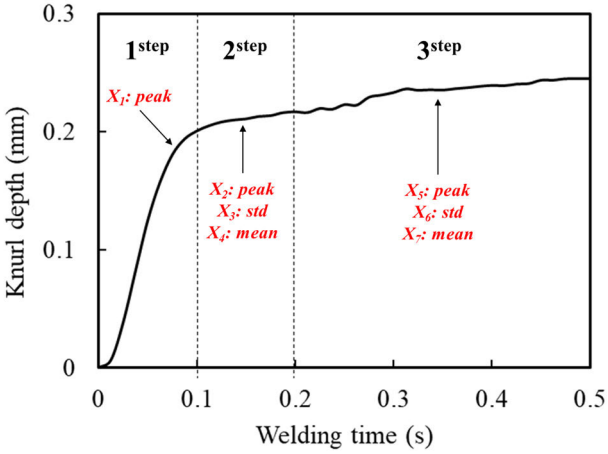

FIGURE 14. Feature variables of LVDT signals.

the knurl depth were selected. For step 3, we selected the peak (X5), std (X6), and mean (X7) values of the knurl depth as feature variables.

In Fig. 15, the output energy extracted from processing the signals using the current and voltage sensors is compared according to the weld quality. As there is an interface between the output energy values of IW, SW, and EW depending on the weld quality, we selected the energy (X8) and welding time (X9) as additional feature variables.

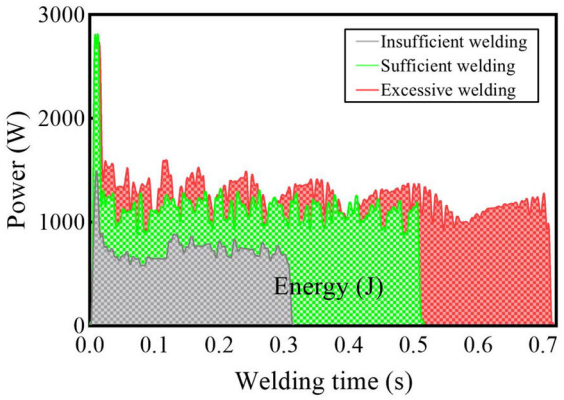

FIGURE 15. Comparison of welding energy according to weld quality.

2) MULTI-CLASS CLASSIFICATION USING SVM FOR WELD QUALITY PREDICTION

To predict the weld quality, we developed an SVM-based classification model by utilizing nine feature variables, including the seven feature variables of the LVDT signal extracted in the previous section and two feature variables for energy and welding time extracted through power signal processing. The nine selected feature variables were set as input values, and the output values were classified into IW (class 0), SW (class 1), and EW (class 2), based on which training and evaluation were performed.

SVM is basically designed for binary classification. However, as multi-class classification is performed in this study, we constructed a multi-class classification system by combining multiple binary classifiers. For this, we built a model using the one-vs.-one (OVO) method, which was developed from among various approaches to combine multiple binary classifiers, as shown in Fig. 16.

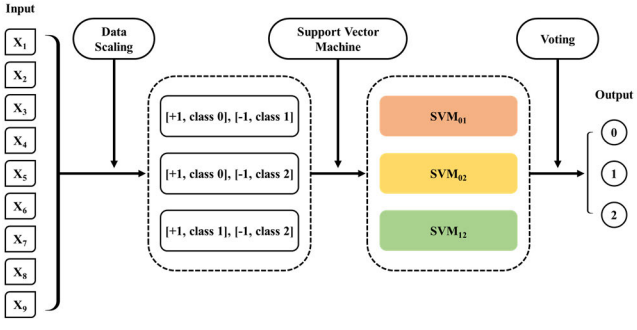

FIGURE 16. Schematic diagram of multi-class classification structure using SVM.

First, we performed scaling of the input data. Furthermore, standardization was performed as shown in Eq. (4), so that the mean and std of each data group would be 0 and 1.

$$\hat{X}_{i,j} = \frac{X_{i,j} - X_{i,mean}}{X_{i,std}} \tag{4}$$

where $X_{i,mean}$ and $X_{i,std}$ are the mean and standard deviation of the input data group of the i-th index, and $X_{i,j}$ is the value of the j-th datapoint in the group. In the OVO method, the number of classifiers is determined by Eq. (5) in multi-class classification with m classes.

$$\text{Number of classifier} = \frac{m(m-1)}{2} \tag{5}$$

As there are three classes in this study, we constructed three classifiers, namely class 0 and class 1, class 0 and class 2, and class 1 and class 2. Of the total 446 data, 264 were classified as class 0, 123 as class 1, and 59 as class 2. In addition, after fitting 134 test datapoints to the three classifiers trained with 312 train datapoints out of a total of 446 datapoints, we constructed a multi-class classification system that returns the most voted label. The SVM kernel used in this study is linear, and for the C-parameter, 10 was used. Finally, the confusion matrix was used as a metric for evaluating the classification model as shown in Fig. 17, and the accuracy was calculated by Eq. (6).

$$\text{Accuracy} = \frac{TP + TN}{TP + TN + FP + FN} \tag{6}$$

		Actual values	
		True	False
Predictive values	True	True Positive (TP)	False Positive (FP)
	False	False Negative (FN)	True Negative (TN)

FIGURE 17. Confusion matrix for classification.

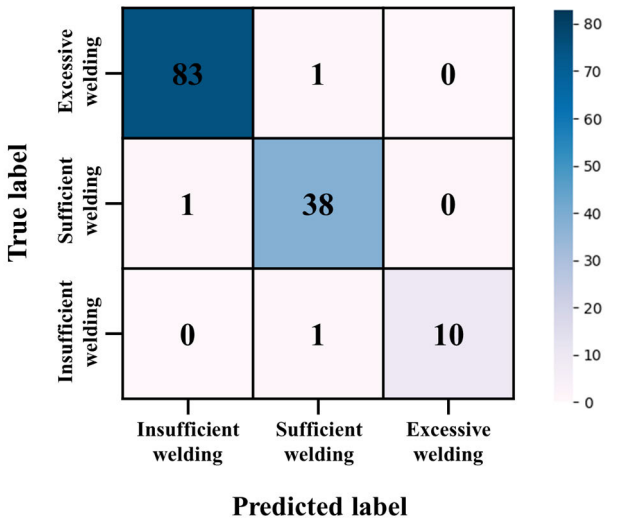

FIGURE 18. Confusion matrix for multi-class classification.

Figure 18 shows the confusion matrix used for a comparative evaluation of the class predicted by the trained SVM

using the test input data and the class of the actual test output data. The accuracy is determined to be approximately 98%.

Finally, the overall flow chart for UMW quality prediction using the current and voltage sensors and the LVDT sensor is shown in Fig. 19. In summary, after acquiring the current, voltage, and LVDT signals generated during welding, we extracted the feature variables for classification through data preprocessing. The extracted feature variables were standardized to create a data set, and the OVO method-based SVM was used to classify and predict the weld quality as IW (class 0), SW (class 1), or EW (class 2).

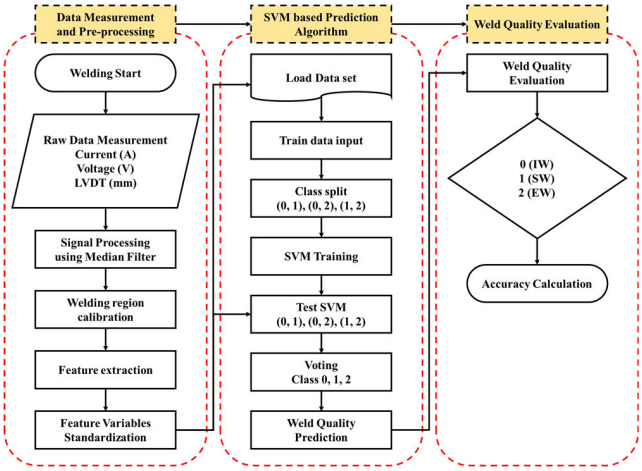

FIGURE 19. Flow chart of weld quality prediction algorithm.

IV. CONCLUSION

In this study, we constructed a system for the monitoring of the UMW process of lithium-ion battery cell materials consisting of a 8-μm-thick Cu foil and a 0.2-mm-thick nickel-plated copper strip using current, voltage, and LVDT sensors. To this end, the algorithm for evaluating and predicting the welding quality was analyzed in a variety of ways. As a result, the following conclusions were obtained:

1) In this study, we proposed a method for real-time monitoring of the UMW process by utilizing sensors. The current and voltage sensors were connected to the secondary output terminals inside the welder controller to obtain data, and the LVDT sensor was mounted on top of the sonotrode to obtain data on the behavior of the knurl depth according to weld time.
2) We presented a method for classifying the weld quality by the processing current, voltage, and LVDT sensor signals. For the current and voltage sensors, we presented a method for converting data into power signals through data processing to derive the welding output energy. For the LVDT sensor, we presented a method of deriving a signal that represents the behavior of the knurl depth during welding time through data processing.
3) We proposed a weld quality prediction algorithm using an SVM-based classification model. Seven features were selected by analyzing the growth patterns of the knurl depth, and two features were selected by calculating the welding output energy and welding time from the power signal. A total of nine features were used as input to the SVM-based classification model, and the output was classified into three classes to predict the weld quality. The test data evaluation results showed a prediction accuracy of approximately 98%.

In the future, this study can be used as a guideline for the development of UMW quality monitoring technology applied to battery cell materials of multilayered foils.

REFERENCES

[1] M. Kii, "Reductions in CO_2 emissions from passenger cars under demography and technology scenarios in Japan by 2050," *Sustainability*, vol. 12, no. 17, p. 6919, Aug. 2020.
[2] P. Siskos, P. Capros, and A. De Vita, "CO_2 and energy efficiency car standards in the EU in the context of a decarbonisation strategy: A model-based policy assessment," *Energy Policy*, vol. 84, pp. 22–34, Sep. 2015.
[3] M. A. Hannan, Md. M. Hoque, A. Hussain, Y. Yusof, and P. J. Ker, "State-of-the-art and energy management system of lithium-ion batteries in electric vehicle applications: Issues and recommendations," *IEEE Access*, vol. 6, pp. 19362–19378, 2018.
[4] A. Adib, K. K. Afridi, M. Amirabadi, F. Fateh, M. Ferdowsi, B. Lehman, L. H. Lewis, B. Mirafzal, M. Saeedifard, M. B. Shadmand, and P. Shamsi, "E-mobility—Advancements and challenges," *IEEE Access*, vol. 7, pp. 165226–165240, 2019.
[5] M. Muratori, M. Alexander, D. Arent, M. Bazilian, P. Cazzola, E. M. Dede, J. Farrell, C. Gearhart, D. Greene, and A. Jenn, "The rise of electric vehicles-2020 status and future expectations," *Prog. Energy*, vol. 3, no. 2, 2021, Art. no. 022002.
[6] E. Biro, D. Weckman, and Y. Zhou, "Pulsed Nd: Yag laser welding of copper using oxygenated assist gases," *Metall. Mater. Trans. A*, vol. 33, pp. 2019–2030, Jul. 2002.
[7] S. S. Lee, T. H. Kim, S. J. Hu, W. W. Cai, and J. A. Abell, "Joining technologies for automotive lithium-ion battery manufacturing: A review," in *Proc. Int. Manuf. Sci. Eng. Conf.*, 2010, pp. 541–549.
[8] L. Lu, X. Han, J. Li, J. Hua, and M. Ouyang, "A review on the key issues for lithium-ion battery management in electric vehicles," *J. Power Sour.*, vol. 226, pp. 272–288, Mar. 2013.
[9] S. J. Lee, H. Nakamura, Y. Kawahito, and S. Katayama, "Effect of welding speed on microstructural and mechanical properties of laser lap weld joints in dissimilar Al and Cu sheets," *Sci. Technol. Weld. Joining*, vol. 19, no. 2, pp. 111–118, Feb. 2014.
[10] N. Nitta, F. Wu, J. T. Lee, and G. Yushin, "Li-ion battery materials: Present and future," *Mater. Today*, vol. 18, no. 5, pp. 252–264, Jun. 2015.
[11] D. Deng, "Li-ion batteries: Basics, progress, and challenges," *Energy Sci. Eng.*, vol. 3, no. 5, pp. 385–418, Sep. 2015.
[12] A. Das, D. Li, D. Williams, and D. Greenwood, "Weldability and shear strength feasibility study for automotive electric vehicle battery tab interconnects," *J. Brazilian Soc. Mech. Sci. Eng.*, vol. 41, no. 1, pp. 1–14, Jan. 2019.
[13] C. Vidal, P. Malysz, P. Kollmeyer, and A. Emadi, "Machine learning applied to electrified vehicle battery state of charge and state of health estimation: State-of-the-art," *IEEE Access*, vol. 8, pp. 52796–52814, 2020.
[14] M. F. R. Zwicker, M. Moghadam, W. Zhang, and C. V. Nielsen, "Automotive battery pack manufacturing—A review of battery to tab joining," *J. Adv. Joining Processes*, vol. 1, Mar. 2020, Art. no. 100017.
[15] M. J. Brand, P. A. Schmidt, M. F. Zaeh, and A. Jossen, "Welding techniques for battery cells and resulting electrical contact resistances," *J. Energy Storage*, vol. 1, pp. 7–14, Jun. 2015.
[16] T. H. Kim, J. Yum, S. J. Hu, J. P. Spicer, and J. A. Abell, "Process robustness of single lap ultrasonic welding of thin, dissimilar materials," *CIRP Ann.*, vol. 60, no. 1, pp. 17–20, 2011.
[17] Y. Y. Zhao, D. Li, and Y. S. Zhang, "Effect of welding energy on interface zone of Al–Cu ultrasonic welded joint," *Sci. Technol. Weld. Joining*, vol. 18, no. 4, pp. 354–360, May 2013.
[18] A. Das, D. Li, D. Williams, and D. Greenwood, "Joining technologies for automotive battery systems manufacturing," *World Electric Vehicle J.*, vol. 9, no. 2, p. 22, Jul. 2018.

[19] K. Arimoto, T. Sasaki, Y. Doi, and T. Kim, "Ultrasonic bonding of multi-layered foil using a cylindrical surface tool," *Metals*, vol. 9, no. 5, p. 505, Apr. 2019.
[20] S. Shin, S. Nam, J. Yu, J. Park, and D. Kim, "Ultrasonic metal welding of multilayered copper foils to nickel-plated copper sheet in lithium-ion battery cell," *Metals*, vol. 11, no. 8, p. 1195, Jul. 2021.
[21] M. de Leon and H.-S. Shin, "Prediction of optimum welding parameters for weld-quality characterization in dissimilar ultrasonic-welded Al-to-Cu tabs for Li-ion batteries," *Met. Mater. Int.*, vol. 29, no. 4, pp. 1079–1094, Apr. 2023.
[22] S. Samir, K. Dave, V. Badheka, and D. Patel, "Optimization of process parameters of ultrasonic metal welding for multi layers foil of AL8011 material," *Weld. Int.*, vol. 37, no. 3, pp. 119–127, Mar. 2023.
[23] G. Tian, C. Yang, X. Lu, Z. Wang, Z. Liang, and X. Li, "Inductance-to-digital converters (LDC) based integrative multi-parameter eddy current testing sensors for NDT&E," *NDT, E Int.*, vol. 138, Sep. 2023, Art. no. 102888.
[24] I. Balz, E. A. Raad, E. Rosenthal, R. Lohoff, A. Schiebahn, U. Reisgen, and M. Vorländer, "Process monitoring of ultrasonic metal welding of battery tabs using external sensor data," *J. Adv. Joining Processes*, vol. 1, Mar. 2020, Art. no. 100005.
[25] S. Shawn Lee, C. Shao, T. Hyung Kim, S. Jack Hu, E. Kannatey-Asibu, W. W. Cai, J. Patrick Spicer, and J. A. Abell, "Characterization of ultrasonic metal welding by correlating online sensor signals with weld attributes," *J. Manuf. Sci. Eng.*, vol. 136, no. 5, Oct. 2014, Art. no. 051019.
[26] Z. Ma and Y. Zhang, "Characterization of multilayer ultrasonic welding based on the online monitoring of sonotrode displacement," *J. Manuf. Processes*, vol. 54, pp. 138–147, Jun. 2020.
[27] W. Guo, C. Shao, T. H. Kim, S. J. Hu, J. J. Jin, J. P. Spicer, and H. Wang, "Online process monitoring with near-zero misdetection for ultrasonic welding of lithium-ion batteries: An integration of univariate and multivariate methods," *J. Manuf. Syst.*, vol. 38, pp. 141–150, Jan. 2016.

HYOJUN CHOI received the B.S. degree in mechanical engineering from Incheon National University, Incheon, South Korea, in 2022. He is currently pursuing the M.S. degree in mechanical engineering with Hanyang University, Seoul, South Korea. His research interests include the application of deep learning to welding processes and mechanical engineering applications, and the development of automation technology for welding monitoring.

SEUNGMIN SHIN received the B.S. degree in mechanical engineering from Hanyang University (ERICA Campus), Ansan, South Korea, in 2007, and the Ph.D. degree in mechanical engineering from Hanyang University, Seoul, South Korea, in 2019. From 2019 to 2020, he was a Postdoctoral Researcher Engineer with the Advanced Welding Laboratory, Hanyang University. He is currently a Principal Research Engineer with LG Energy Solution, Daejeon, South Korea. His research interests include the automation of welding monitoring systems and welding technology.

DONG-YOON KIM received the B.S. degree in electrical engineering from Dongseo University, Busan, South Korea, in 2009, and the M.S. degree in mechanical engineering from Pukyong National University, Busan, in 2012. He is currently pursuing the Ph.D. degree in mechanical engineering with Hanyang University, Seoul, South Korea. His research interests include the development of welding and manufacturing processing, and welding and joining technologies.

JIYONG PARK received the B.S. and M.S. degrees in mechanical engineering from Hanyang University, Seoul, South Korea, in 2008 and 2010, respectively, and the Ph.D. degree in mechanical engineering from the Korea Advanced Institute of Science and Technology, Daejeon, South Korea, in 2017. He is currently a Principal Research Engineer with the Korea Institute of Industrial Technology, Incheon, South Korea. His research interests include additive manufacturing, laser welding, and heat treatment.

DONGCHEOL KIM received the B.S., M.S., and Ph.D. degrees in mechanical engineering from Hanyang University, Seoul, South Korea, in 1993, 1995, and 2000, respectively. He is currently a Principal Research Engineer with the Korea Institute of Industrial Technology, Incheon, South Korea. His research interests include the development of welding and manufacturing processing, arc physics, and welding and joining technologies.

SEUNG HWAN LEE received the B.S. degree in mechanical engineering from Hanyang University, Seoul, South Korea, in 2004, and the M.S. and Ph.D. degrees in mechanical engineering from the University of Michigan, Ann Arbor, MI, USA, in 2007 and 2013, respectively. From 2013 to 2014, he was a Chief Researcher Engineer with Sensigma LLC, Ann Arbor, MI, USA. He is currently an Associate Professor with Hanyang University. His research interests include laser physics, laser welding, additive manufacturing, and deep learning.

JIYOUNG YU received the B.S. and Ph.D. degrees in mechanical engineering from Hanyang University, Seoul, South Korea, in 2007 and 2013, respectively. From 2013 to 2019, he was a Principal Research Engineer with Hyundai Steel Company, Dangjin, South Korea. He is currently a Principal Research Engineer with the Korea Institute of Industrial Technology, Incheon, South Korea. His research interests include the automation of welding systems and welding and joining technologies.